metals

MDPI

Article

Investigation of Residual Stress Distribution and Fatigue of 7050-T7451 Alloy Hole Components with Laser Shock and Ultrasonic Extrusion

Yinfang Jiang [1,2,*], Xiancheng Liu [1,*], Yangyang Wang [1], Lingling Cui [2], Guang Ji [2] and Wei Liu [1]

[1] School of Mechanical Engineering, Jiangsu University, Zhenjiang 212000, China
[2] School of Mechanical Engineering, Nantong Institute of Technology, Nantong 226000, China
* Correspondence: yfjiang@ujs.edu.cn (Y.J.); 2212103038@stmail.ujs.edu.cn (X.L.); Tel.: +86-139-1456-7669 (Y.J.); +86-178-2607-3910 (X.L.)

Abstract: Small-hole structures, such as the millions of fastener holes found on aircraft, are typical stress-concentration structures prone to fatigue failure. To further improve the strengthening process of this small-hole structure, we make up for the limitations of laser shock processing (LSP) of small holes by combining it with the ultrasonic extrusion strengthening (UES) process to form a new strengthening method—laser shock and ultrasonic extrusion strengthening (LUE). The influence of the LUE process sequence and process parameters on residual stress distribution was studied through FEM, and the gain of fatigue life of specimens after LUE strengthening was also explored through tests. The results show that when using LUE technology, the friction force decreases with the increase in amplitude and decreases by 3.2% when the amplitude is maximum. The LUE process eliminates the thickness effect generated by LSP, which can achieve good stress distribution of small-hole components under smaller laser shock peak pressure, and reduces equipment power. LUE can significantly improve the fatigue life of small-hole components, and the maximum fatigue life gain can be up to 310.66%.

Keywords: laser shock processing; ultrasonic extrusion; combined strengthening; small-hole components; fatigue test

check for updates

Citation: Jiang, Y.; Liu, X.; Wang, Y.; Cui, L.; Ji, G.; Liu, W. Investigation of Residual Stress Distribution and Fatigue of 7050-T7451 Alloy Hole Components with Laser Shock and Ultrasonic Extrusion. *Metals* **2024**, *14*, 597. https://doi.org/10.3390/met14050597

Academic Editor: Roland Logé

Received: 24 April 2024
Revised: 12 May 2024
Accepted: 16 May 2024
Published: 19 May 2024

Copyright: © 2024 by the authors. Licensee MDPI, Basel, Switzerland. This article is an open access article distributed under the terms and conditions of the Creative Commons Attribution (CC BY) license (https://creativecommons.org/licenses/by/4.0/).

1. Introduction

As the power system of an airplane, the aero-engine is known as the "pearl on the crown of modern industry". However, due to its high speed, high temperature, vibration, and long working hours, the small-hole connecting parts of the aero-engine are prone to high-cycle fatigue fracture in harsh working environments [1], which seriously affects the safety and reliability of the engine. To solve this problem, scientists and engineers have been exploring new strengthening technologies [2,3].

Mandrel extrusion technology is commonly used to strengthen small-diameter hole structures. It makes the hole wall produce elastic–plastic deformation and residual compressive stress by extruding the mandrel into a slightly narrower hole [4,5]. However, in some cases, the mandrel directly contacts the hole wall, and the friction and pulling force between them are large. The plastic flow of the hole wall surface metal is serious, which can cause scratches on the hole wall surface and mandrel fracture [6–8]. Liu et al. [9] and Han et al. [10], respectively, studied the effect of ultrasound on hole machining and micro-extrusion, and the results showed that the addition of ultrasound vibration reduced friction, improved surface roughness of the workpiece, and made the strengthening effect better. Mousavi et al. [11] studied the ultrasonic extrusion process, and numerical simulation results showed that applying ultrasonic vibration during conventional extrusion can reduce the static pressure and yield stress of the material. However, this method has no significant effect on the plastic strain of the material. Laser shock processing, an emerging

strengthening technology, has been widely used to strengthen small-hole connecting parts in aviation structures [12–15]. LSP strengthens the material surface to regulate the stress distribution on the inner wall of the small hole [15,16] by pre-setting residual compressive stress and improving the microstructure, LSP significantly improves the high-cycle fatigue performance of metal materials [17]. However, when applied to hole structures in thicker plates, the depth of the residual compressive stress layer induced by laser shock processing (LSP) is insufficient, resulting in residual tensile stresses even in the middle of the hole wall, which produces a thickness effect, thus limiting the fatigue life of the workpiece [18,19]. To overcome the existing limitations of LSP-reinforced small-hole components, we combined ultrasonic extrusion strengthening (UES) with LSP to form a new strengthening method—laser shock processing and ultrasonic extrusion (LUE). We have performed relevant exploratory research on the improvement of the strengthening effect brought by LUE [20]. However, there are still some problems that need to be solved in the current LUE process; for example, studies have not yet explored whether the process sequence in the LUE process will have an effect on the strengthening effect and have not examined the effect of process parameters such as peak pressure, amplitude, and extrusion ratio of the LUE on the distribution of residual stresses.

In this study, the small-hole structure of the 7075-T7451 aluminum alloy was used as the research object, and the effects of the LUE process sequence, peak pressure, amplitude, and extrusion ratio on the residual stress distribution of the LUE process were investigated by finite element analysis and verified by the fatigue test.

2. Materials and Methods

2.1. Specimens and Material Parameters

In this study, the specimen selected was the 7050-T7451 aluminum alloy (Shanghai Chuangyue Metal Group, Shanghai, China) duplex small-hole specimen. The material parameters are listed in Table 1, and the chemical composition parameters are listed in Table 2. The geometric dimensions are shown in Figure 1.

Table 1. Material parameters of 7050-T7451 aluminum alloy.

Material	Density/(kg/m^3)	Yield Strength/MPa	Poisson's Ratio	Elastic Modulus/GPa
7050-T7451	2830	441	0.33	69

Table 2. Chemical composition of 7050-T7451 aluminum alloy.

Plate No.	Si	Fe	Cu	Mn	Mg	Cr	Zr	Zn	Ti	Al
7050 (wt%)	0.12	0.15	2.0–2.6	0.10	1.9–2.6	0.04	0.08–0.15	5.7–6.7	0.06	Remainder

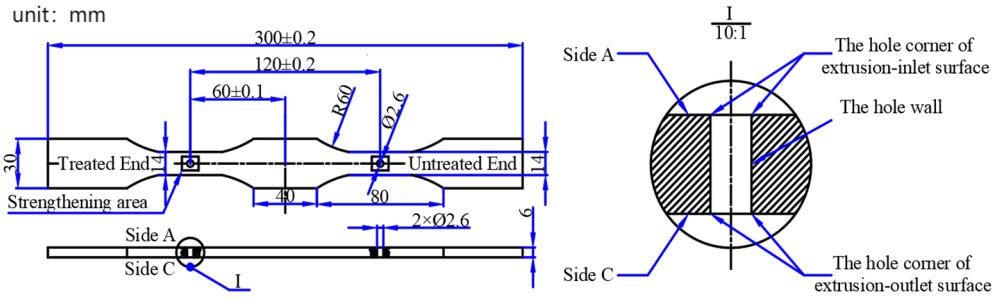

Figure 1. The specimen's geometric dimension drawing.

2.2. Establishment of LUE Finite Element Model

This study used two LUE methods for finite element analysis, and the difference between the two methods was related to processing. LUE-1: 1. Opening holes; 2. Ultrasonic

extrusion—making the mandrel that undergoes ultrasonic vibration pass through the small hole at a uniform speed; and 3. Laser peening—the model and parameter settings are consistent with the ultrasonic extrusion described above, and an anti-deformation mandrel is added to the simulation model to limit the deformation of the hole corner during laser peening. LUE-2: 1. Laser peening—define the hole area as a "birth–death element set" named "Kong"; 2. Opening holes: removing the "Kong" element set; and 3. Ultrasonic extrusion—making the mandrel pass through the small hole at a uniform speed, and the initial residual stress field should be the stable residual stress field inside the material after laser peening strengthening.

2.2.1. LUE-1: Finite Element Model Establishment

The ultrasonic extrusion mandrel (Hangzhou Chenggong Ultrasonic Co., Ltd., Hangzhou, China) is a key tool for implementing the ultrasonic extrusion strengthening process. Its structure is shown in Figure 2 and includes a guide section, front cone section, rear cone section, working ring, and tail end. When extruding aluminum-alloy small holes, the anterior cone angle α is 2.5° to 3.5°, and the posterior cone angle β is 4° to 4.5°. The working segment is the part that directly and effectively extrudes the small hole. Its length, b, is 0.8 mm, and its diameter is d. The relative extrusion ratio (Er) is $(d - d_0)/d_0$ (d_0 is the diameter of the hole). The mandrel material is a tungsten–molybdenum high-speed steel with an elastic modulus, E, of 210 Gpa, a Poisson's ratio of 0.3, and a density of 7.85 g/cm^3.

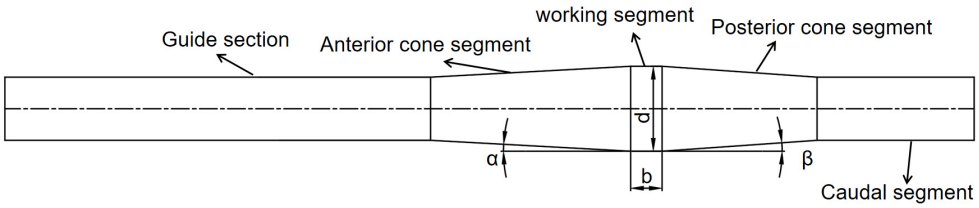

Figure 2. Structure diagram of ultrasonic extrusion mandrel.

During the meshing process of the mandrel, the working segment part is refined because it directly contacts the inner surface of the small hole, while the mesh size of the guide section and caudal end can be larger. The meshing is shown in Figure 3b. During the ultrasonic extrusion process, the inner wall of the small hole and the outer surface of the anterior cone section, posterior cone section, and working segment of the mandrel are in contact with each other, and the contact mode is face-to-face contact. Compared to the mandrel material, i.e., tungsten–molybdenum high-speed steel, the aluminum alloy has lower strength and stiffness. The contact process is a contact between a soft material and a hard material. According to the ABAQUS contact setting principle, the outer surface of the mandrel is set as the master surface, and the inner surface of the small hole is set as the slave surface. During the actual extrusion strengthening process, the outer surface of the mandrel and the inner surface of the small hole are both pre-treated to ensure their surface quality. Lubricants with good lubrication effects such as molybdenum disulfide and calcium-based grease are used. Therefore, the friction coefficient is set to $\mu = 0.05$ during the simulation process [11].

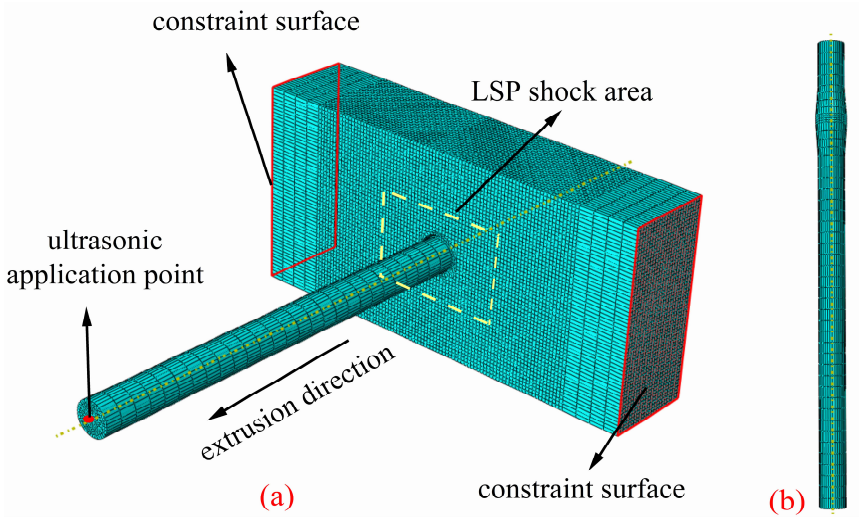

Figure 3. LUE-1 finite element model: (**a**) grid division and load boundary condition setting and (**b**) mandrel grid division.

The size of the finite element model of aluminum-alloy small-hole structure established to simplify the model is 28 mm × 14 mm × 6 mm. The meshing type of the aluminum-alloy small-hole structure and CET is the 8-node linear brick (C3D8) element [21], which has better deformation performance and better stress-solving ability. In the process of meshing, the grid length at both ends of the model, which is far from the laser peening impact area, is set to 1 mm, and the grid length in the area near the small hole is set to 0.25 mm. The meshing is shown in Figure 3a. During the simulation process, the aluminum-alloy small-hole structure was constrained to remain stationary. The mandrel was set to enter the hole from the extrusion-inlet surface and extrude from the extrusion-outlet surface at a speed of 1 mm/s during the strengthening process. During this process, the mandrel undergoes ultrasonic vibration, which is applied to the vertex of the mandrel and propagates along the axis of the mandrel, causing the mandrel to produce longitudinal ultrasonic vibration, as shown in Figure 3a. In this study, the initial phase angle is set to 0, and the vibration of the mandrel varies according to a sinusoidal law, with a mathematical expression of:

$$S = Bsin(2\pi ft), \tag{1}$$

where S is the displacement of the mandrel, B is the amplitude, f is the frequency, and t is the time. Due to the extremely small diameter of the mandrel, it is currently required to achieve its inherent frequency of ultrasonic vibration in actual experiments; so, the frequency variation is temporarily not considered. Through modal analysis, the frequency 17.537 KHz is derived as the frequency of mandrel vibration.

After ultrasonic extrusion, the initial residual stress field of laser peening should be the stable residual stress field inside the material after UES, and an anti-deformation mandrel should be added, as shown in Figure 4b. The other parameters of the simulation model are consistent with those described above. The side of the model is set as a constraint surface, and the constraint method is a full constraint to ensure the fixation of the small-hole structure and make it consistent with the conditions of actual experiments. The LSP overlay rate is 50%, and the pressure size of the laser-induced shock wave follows a Gaussian distribution trend throughout the entire time it acts on the material, and the pressure load curve that changes with time is shown in Figure 4a [22]. In the LSP simulation process, this paper uses the Johnson–Cook constitutive model [23], which does not consider temperature effects. The expression of the Johnson–Cook model can be simplified as:

$$\sigma_y = (A + B\varepsilon^n)\left[1 + CLn\left(1 + \frac{\varepsilon'}{\varepsilon_0}\right)\right], \tag{2}$$

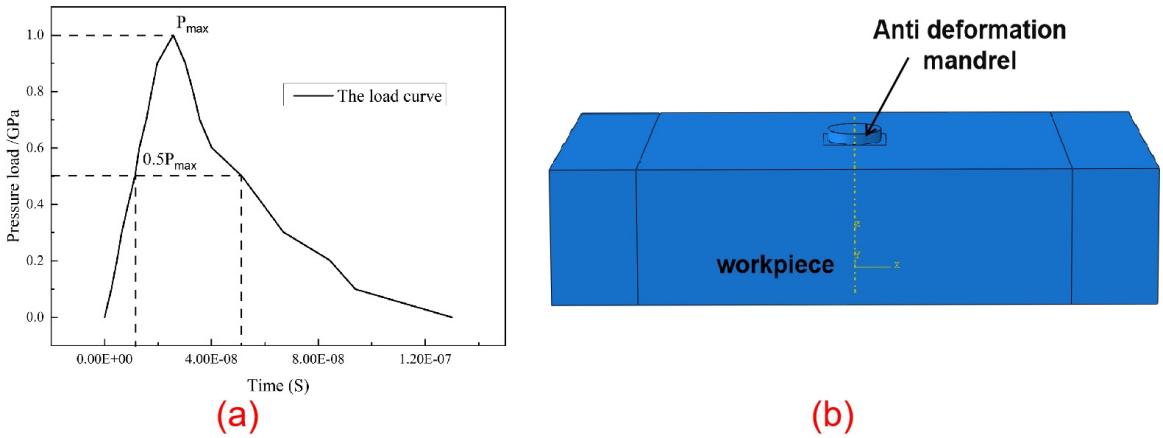

Figure 4. (**a**) LSP load curve and (**b**) model with added anti-deformation mandrel.

In the equation, σ_y represents the yield stress, A represents the yield strength, which is determined by the yield stress and hardening coefficient of the material, B represents the hardening coefficient, which is determined by the deformation stress and deformation rate of the material, ε' represents the plastic strain, ε_0 represents the strain rate, n is the hardening coefficient, and C is the strain rate sensitivity coefficient. The parameters of the Johnson–Cook model are shown in Table 3.

Table 3. Parameters of Johnson–Cook model of 7050-T7451.

Material	A	B	C	n
7050-T7451	0.441 GPa	0.177344 GPa	0.02	0.33583

2.2.2. LUE-2: Finite Element Model Establishment

The model size parameters and the grid division scheme are the same as in LUE-1. The difference lies in the pre-treatment of the unperforated specimen with laser peening, as shown in Figure 5a. The use of the "life–death" element method replaces the perforation process, with the set of hole elements to be removed designated as "Kong", and modifications made in the corresponding keywords of the analysis steps to affect their removal. Subsequently, ultrasonic extrusion is performed, with the initial residual stress field expected to be the stable residual stress field within the material after laser peening. The ultrasonic extrusion settings are the same as those in Figure 3.

In this post-processing, four paths were extracted, as shown in Figure 5b: A–F is the extrusion-inlet surface path, A–B–C is the hole wall path, C–D is the extrusion-outlet surface path, and B–E is the hole wall middle radial path.

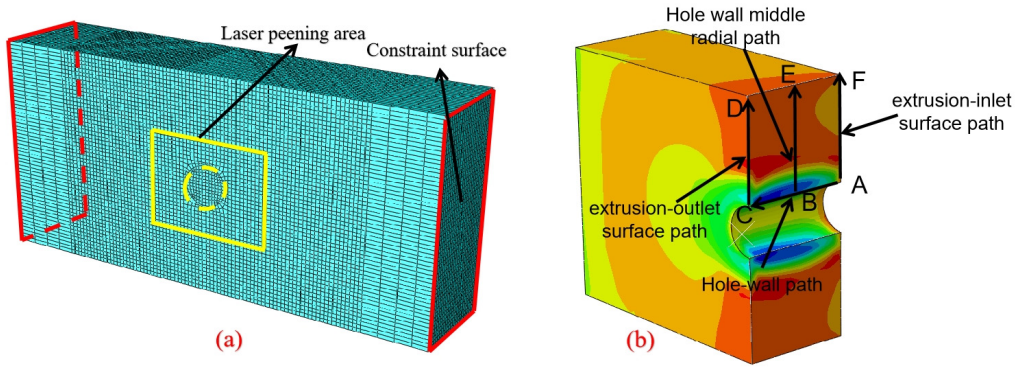

Figure 5. (**a**) LUE-2 finite element model and (**b**) four paths of residual stress distribution analysis.

2.3. LUE-1 Test

Based on the theoretical analysis and numerical analysis results presented earlier, experimental validation of the effectiveness of LUE-1 strengthening was conducted. The test compared the effects of single LSP and the LUE-1 process. The LUE-1 process is illustrated in Figure 6. Initially, the specimen underwent ultrasonic extrusion (Hangzhou Chenggong Ultrasonic Co., Ltd., Hangzhou, China), followed by the addition of an anti-deformation mandrel (the material is consistent with the extrusion mandrel), which was interference-fitted with the small hole. Finally, the laser peening process was performed using double-sided impact with one layer on each side. The laser equipment (THALES, La Défense, France) is shown in Figure 7a. During the test, uniformly flowing pure water served as the confinement layer, and aluminum foil acted as the absorption layer (with a thickness of approximately 0.1 mm). The diameter range of the spot was between 2 mm and 3 mm, with a 50% overlap ratio. The shock path and spot are illustrated in Figure 7b. The peak pressure was set to 2.6 GPa and 4.5 Gpa, the extrusion ratio to 3%, and the amplitude to 8 μm. For this test, four duplex specimens were selected and labeled as C1 to C5. Fatigue tests were conducted after the completion of the LSP and LUE-1 experiments.

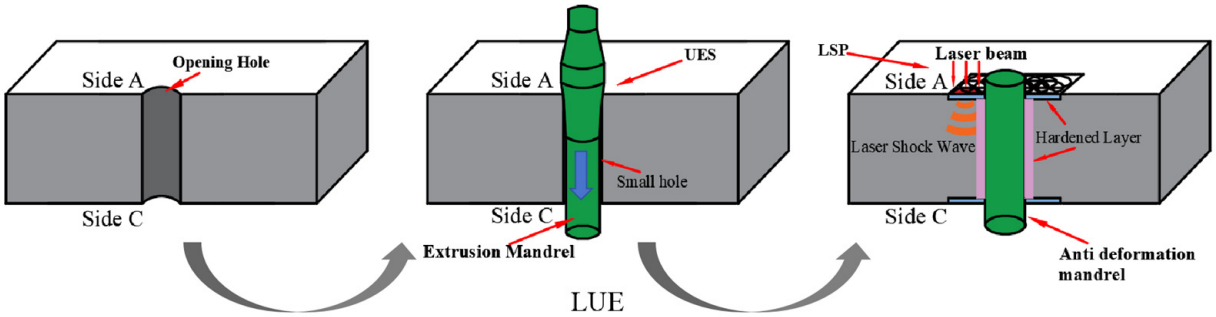

Figure 6. LUE-1 test schematic diagram.

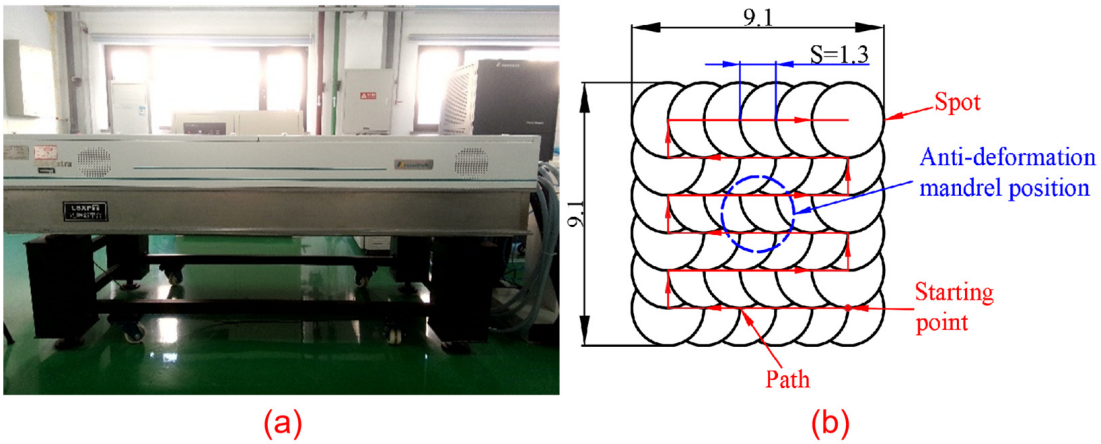

Figure 7. (**a**) LSP equipment and (**b**) LSP shock path.

2.4. Fatigue Test

After the completion of the LUE-1 test, fatigue tensile tests (Technology Co., Ltd., Wuxi, China) were conducted on the duplex specimens with small holes, as shown in Figure 8a,b. The fatigue test employed axial loading with a pull–pull sinusoidal load curve, as depicted in Figure 8c, and the specimen after fracture is shown in Figure 8d. The fatigue test parameters were as follows: stress ratio R = 0.1, frequency f = 40 Hz, and maximum stress σ_{max} = 195 MPa. The specimen clamping method and load curve are shown in the following figure. After one end of the specimen was broken, the fatigue test was continued on the other end.

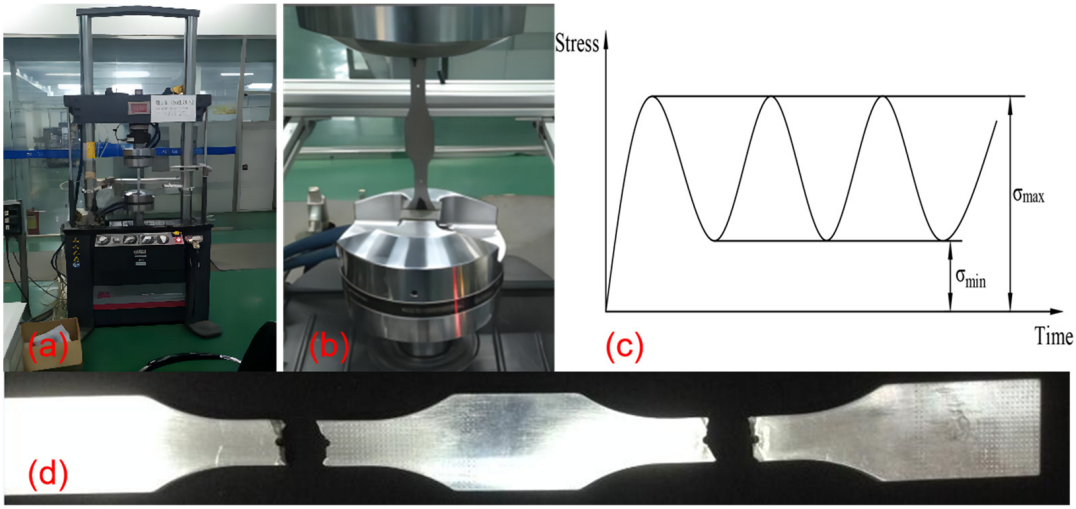

Figure 8. (**a**) Fatigue testing machine; (**b**) sample clamping diagram; (**c**) load curve; and (**d**) a fractured specimen.

3. Results and Analysis

3.1. Influence of Process Methods on Residual Stress Distribution in LUE

The process parameters simulated in this section are peak pressure of 4 GPa, extrusion ratio of 3%, amplitude of 8 μm, and impact mode of double-sided impact. The effect of the LUE process sequence on strengthening is LUE-1. No machining is performed on the holes after both combined and non-combined strengthening treatments. Unless otherwise specified, the parameters in the following text shall remain consistent with this section.

From Figure 9a, the residual compressive stress at the corner of the hole after LSP treatment on the extrusion-inlet surface is the largest, and the radial range (LSP shock zone) of residual compressive stress is larger than that of UES. Both LUE-2 and single UES treatments result in residual tensile stresses on the extrusion-inlet surface, but the peaks and depths of residual stresses in LSP-UES show less variation compared to LSP. For the extrusion-inlet surface, the single UES treatment is the least effective among the four strengthening methods. After LUE-1 treatment, the residual compressive stress within a range of 2 mm from the hole corner of the extrusion-inlet surface is slightly smaller than LSP, but beyond the range, the effectiveness of LUE-1 is superior to the other three strengthening methods. According to Figure 9b, it is known that after LSP treatment, the entire symmetrical region within 1.8 mm from the center of the hole wall exhibits residual tensile stress, and the residual compressive stress at the hole corner is the largest among all the strengthening methods. However, after LUE-2 treatment, the distribution of residual stress on the hole wall is similar to that of single UES treatment, with slightly higher residual compressive stress values. After LUE-1 combined strengthening treatment, the hole wall exhibits only residual compressive stress, and the peak compressive stress generated by LSP is "eliminated" by UES. Furthermore, the residual compressive stress at the hole corner is slightly smaller than that of single LSP treatment but is still relatively large. Therefore, in terms of the hole wall path, the strengthening effect of LUE-1 is superior. According to Figure 9c, it can be observed that among the four strengthening methods on the extrusion-outlet surface path, the surface residual compressive stress is the smallest after single UES treatment, and the residual stress distribution of LSP, LUE-2, and LUE-1 is relatively consistent, indicating that LUE compensates for the shortcomings of single UES treatment. According to Figure 9d, as long as the UES process exists, there is a certain depth of residual compressive stress in the radial direction of the hole, which also compensates for the shortcomings of single LSP.

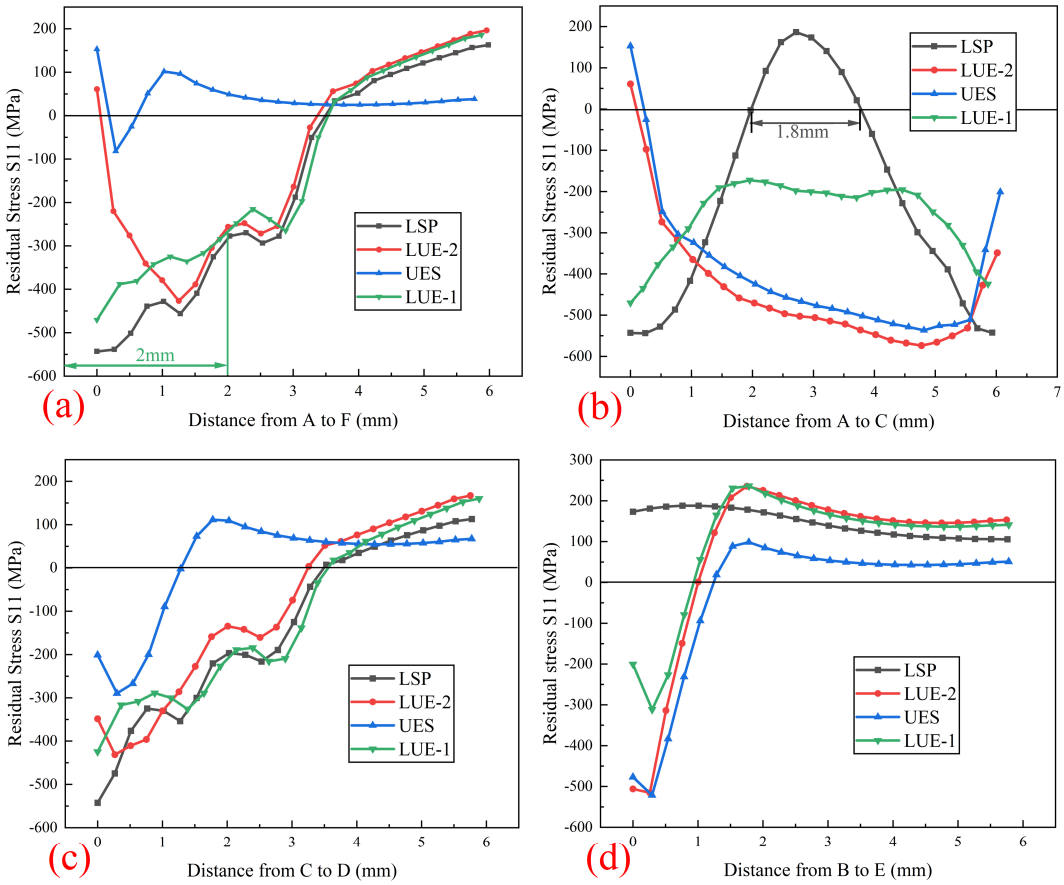

Figure 9. Simulation results of stress distribution of LUE under different process sequences: (**a**) extrusion-inlet surface; (**b**) hole wall path; (**c**) extrusion-outlet surface; and (**d**) hole wall middle radial path.

Based on the comprehensive analysis, it can be concluded that residual tensile stresses exist at the hole corner of the extrusion-inlet surface as long as the final process involves UES. This is due to the plastic flow of the material under the action of the mandrel, where the material at the hole corner of the extrusion-inlet surface is squeezed into the hole, resulting in residual tensile stresses at the hole corner of the extrusion-inlet surface. Therefore, after the UES is completed, the laser peening treatment will cause the tensile stresses in the hole corner of the extrusion-inlet surface to be eliminated and will also cause the residual compressive stresses in the hole corner of the extrusion-outlet surface to be further increased. So, LUE processes are superior to single UES or single LSP. The strengthening effect of LUE-1 is better than that of LUE-2.

3.2. Influence of Peak Pressure on Residual Stress Distribution in LUE-1

The influence of single LSP on residual stresses in the hole wall under different peak pressures is depicted in Figure 10. When the peak pressure reaches 2.6 GPa, the residual stress in the hole corner reaches a saturated state and no longer undergoes significant changes with increasing peak pressure. Prior to 3.5 GPa, increasing the peak pressure gradually reduces the tensile stress in the middle of the hole wall, and the depth of the laser peening effect increases from 1.47 mm to 2.33 mm. It is not until 4.5 GPa that the tensile stress in the middle of the hole wall completely transforms into compressive stress. This indicates that for single LSP strengthening of small-hole structures, achieving relatively ideal results in practical applications requires high-power laser equipment due to the material thickness. LUE-1 will be designed to address this issue.

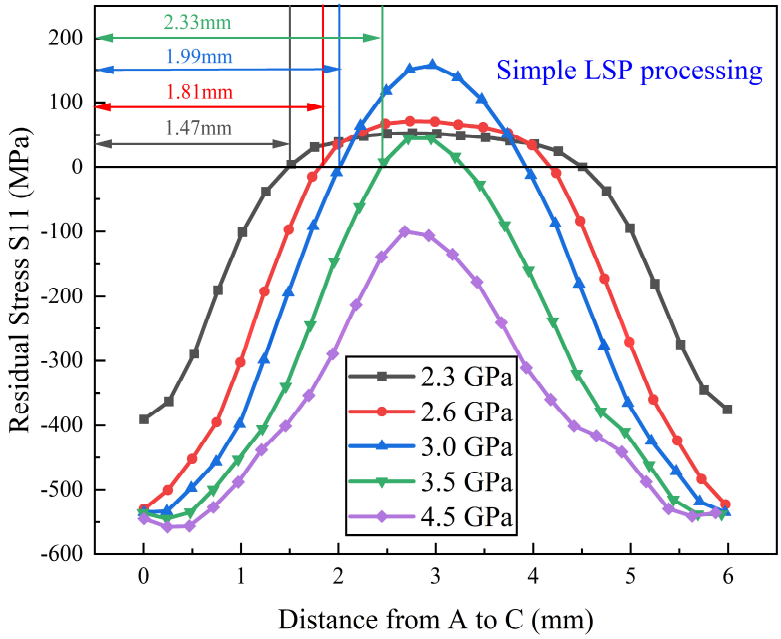

Figure 10. Simulation results of residual stress distribution on hole wall under different peak pressures.

Based on Figure 11a, it is evident that laser peening has a minimal impact on LUE-1 when applied to the extrusion-inlet surface at a peak pressure of P = 1 GPa. Ultrasonic extrusion predominantly governs the process as at a peak pressure of 1 GPa, LSP is slightly higher than the material's fatigue limit, resulting in negligible plastic deformation. However, as the pressure increases to 2 GPa, 3 GPa, 4 GPa, 5 GPa, and 6 GPa, a noticeable downward shift in the residual stress curve is observed, indicating the gradual dominance of laser peening in the LUE-1 process. At peak pressures of 4 GPa, 5 GPa, and 6 GPa, the differences in residual stress peaks are not significant, and the radial distribution range of residual compressive stress on the surface of the small hole gradually increases. The strengthening effect is relatively good and economical at a peak pressure of 4 GPa. According to Figure 11b, along the hole wall path, laser peening has minimal impact on the residual stress field of LUE-1 at a pressure of P = 1 GPa. With a gradual increase in peak pressure, the residual stress at the hole corner gradually increases. The residual stress curve at P = 2 GPa is a "double camel peak" and the residual compressive stress is relatively small. At a pressure of 3 GPa, the residual compressive stresses in the corners of the holes increase further, and the compressive stresses in the middle of the hole wall decrease in comparison. For pressures greater than 4 GPa, the residual stress at the hole corner tends to "saturate". Within a certain range in the middle of the hole wall, the residual stress curve is entirely below the zero line, and with increasing peak pressure, the curve gradually shifts upward, and the tip of the curve becomes sharper. The minimum residual compressive stress reaches −120 MPa. From the perspective of the hole wall, the strengthening effect is relatively ideal at peak pressures of 3 GPa and 4 GPa. As per Figure 11c, on the extrusion-outlet surface path, the residual stress distribution curve shifts downward, and the radial distribution range gradually increases with increasing peak pressure. The differences at 4 GPa, 5 GPa, and 6 GPa are not significant when viewed from the extrusion-outlet surface. According to Figure 11d, along the radial path in the middle part, the residual stress–radial position curve gradually shifts upward, indicating a gradual decrease in residual compressive stress with increasing peak pressure. The differences in residual stress distribution at peak pressures of 4 GPa, 5 GPa, and 6 GPa are not significant.

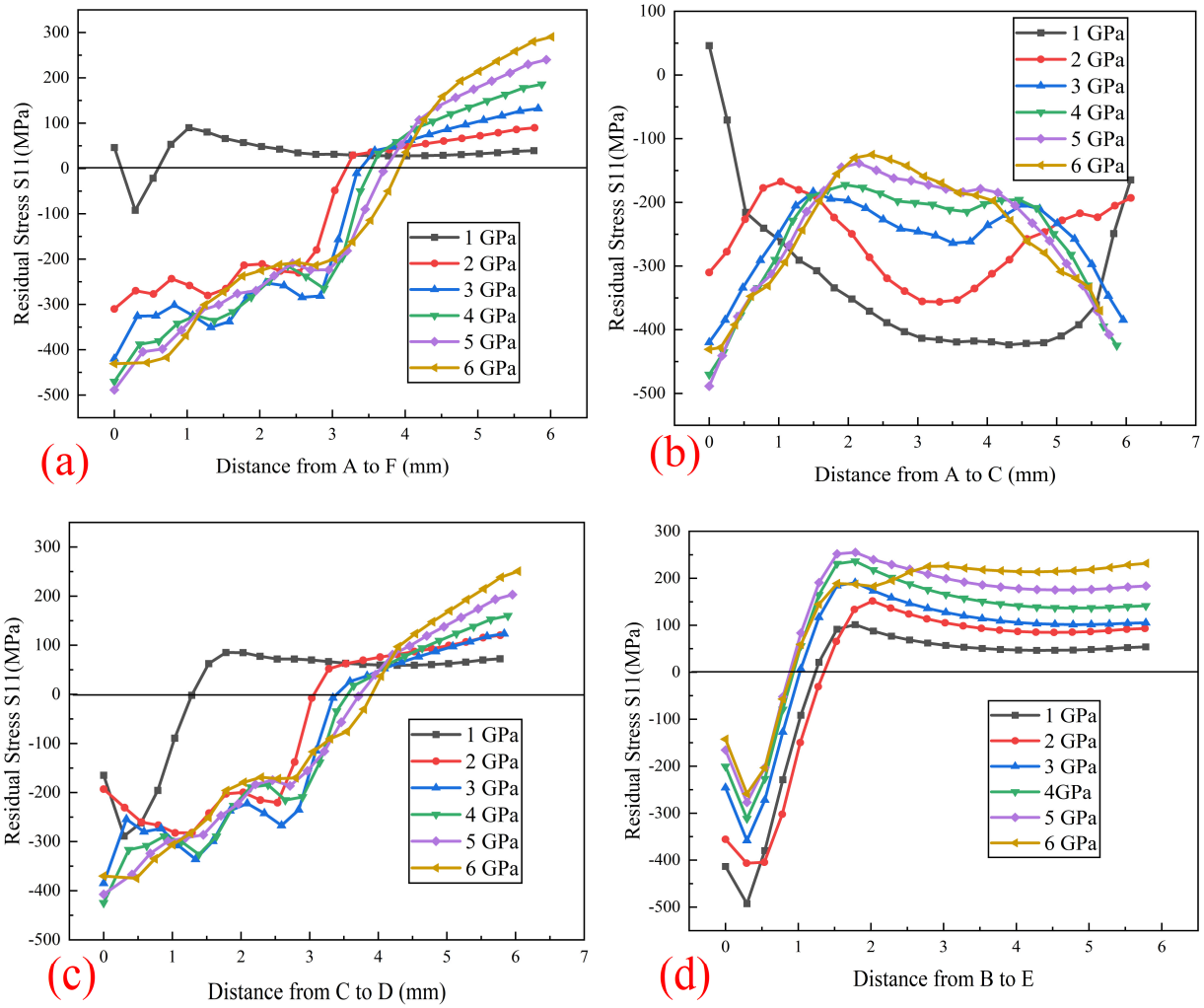

Figure 11. Simulation results of stress distribution of LUE-1 under different peak pressures: (**a**) extrusion-inlet surface; (**b**) hole wall path; (**c**) extrusion-outlet surface; and (**d**) hole wall middle radial path.

Based on Figures 10 and 11, a comparison of the peak stress after LSP treatment and LUE-1 treatment of the hole wall path is plotted, as shown in Figure 12. When using the LUE-1 process, a peak pressure of 2 GPa results in a well-developed residual compressive stress layer on the hole wall, and when the peak pressure P is between 2 and 6 GPa after LUE-1 treatment, the peak stress on the hole wall is all residual compressive stress, with stress values much lower than those from LSP treatment. The LUE-1 process eliminates the thickness effect produced by LSP, enabling small-hole components to achieve a favorable stress distribution at lower laser peak pressures, thus reducing equipment power requirements. Taking into account the effectiveness and cost factors, the recommended ranges for the two processes are shown in Figure 12.

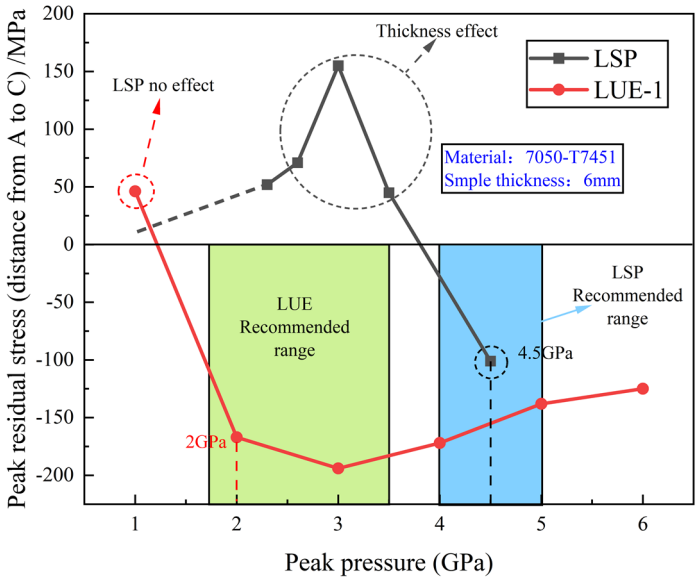

Figure 12. Comparison of peak stress of single LSP and LUE-1 on hole wall path.

3.3. Influence of Amplitude on Residual Stress Distribution in LUE-1

The residual stress distribution of the four paths of the small-hole structure after LUE-1 under different amplitudes is shown in Figure 13, in which it can be seen that the effect of amplitude on the residual stress distribution of LUE-1 is mainly reflected in the middle position of the hole wall surface, and the stress curves overlap when the amplitude is 2 μm, 4 μm, and 6 μm with insignificant changes, and the residual stress values become larger when the amplitude is increased to 8 μm and 10 μm, which is supposed to be due to the fact that the ultrasonic vibration makes the mandrel act on the hole wall several times, thus increasing the plastic deformation of the hole wall [24]. The residual stress distribution at the corners of the holes also changes, but the changes are small and insignificant; overall, the amplitude has a small effect on the LUE-1 stress distribution.

Mechanical properties are an important consideration in the LUE-1 process. Due to the extremely slender nature of the mandrel, excessive tensile force will inevitably lead to mandrel fracture, while excessive frictional force can result in increased power consumption and heat generation. The anti-friction and load-reducing effect of ultrasonic vibration can reduce the frictional force during extrusion, and the reduction of frictional force will lead to a decrease in tensile force. In order to study the influence of different amplitudes on frictional force, the parameters used in this simulation are as follows: peak pressure is 3 GPa, pulse width is 20 ns, relative extrusion ratio is 4%, and ultrasonic amplitudes are 2 μm, 4 μm, 6 μm, 8 μm, and 10 μm, with other parameters remaining the same as in the previous text.

After the simulation is completed, the friction force data are extracted when the working segment completely enters the small hole, and a comparison chart of the friction force for different amplitudes is plotted, as shown in Figure 14. From the graph, it can be observed that as the amplitude increases, the friction force gradually decreases. When the amplitude is 2 μm, the maximum friction force is 547.52 N. For amplitudes of 4 μm, 6 μm, and 8 μm, the maximum values are 542.61 N, 540.32 N, and 533.71 N, respectively. When the amplitude reaches 10 μm, the maximum friction force decreases to 530.18 N. Additionally, with the increase in ultrasonic amplitude, the fluctuation amplitude of the friction force also gradually increases. It can be seen from the graph that when the amplitude is 10 μm, the friction force fluctuates extremely, effectively reducing the friction and load.

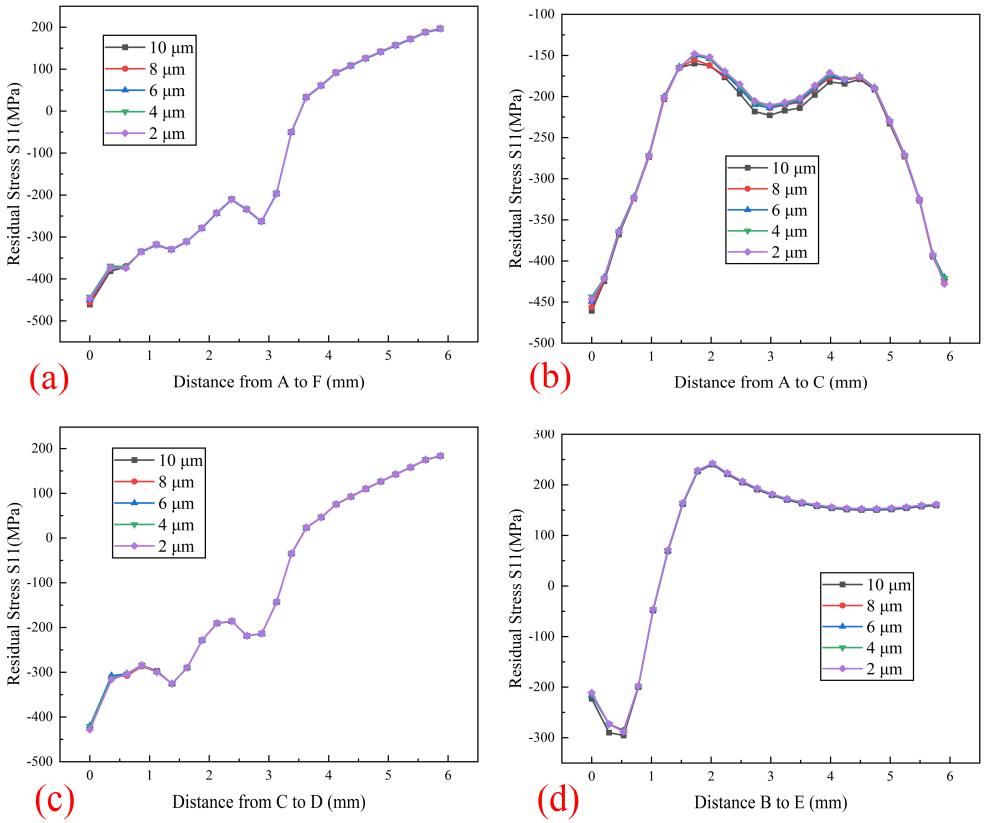

Figure 13. Simulation results of stress distribution of LUE-1 under different amplitudes: (**a**) extrusion-inlet surface; (**b**) hole wall path; (**c**) extrusion-outlet surface; and (**d**) hole wall middle radial path.

Based on the obtained data, the average friction force under different amplitudes during the process is calculated. When the amplitude sequentially increases from 2 μm to 10 μm, the average friction force is 352.23 N, 347.51 N, 324.33 N, 308.73 N, and 283.89 N, respectively. Compared to the average friction force at an amplitude of 2 μm, the average friction force at amplitudes of 4 μm to 10 μm decreases by 1.36%, 8.61%, 14.09%, and 24.07%, respectively.

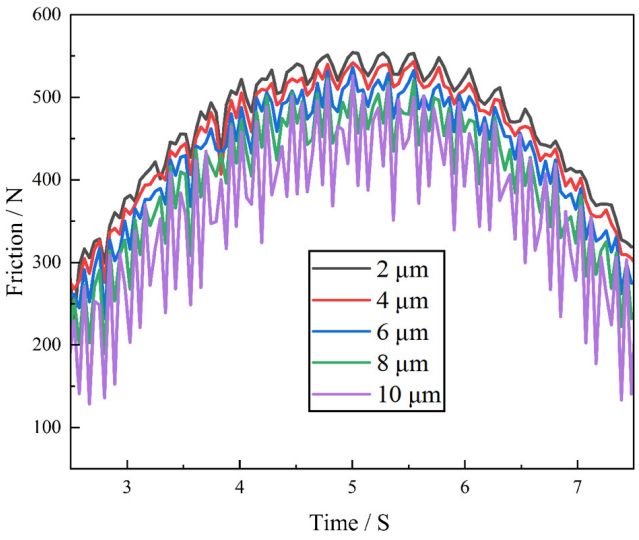

Figure 14. Comparison of friction simulation results at different amplitudes.

3.4. Influence of Extrusion Ratio on Residual Stress Distribution in LUE-1

Aluminum alloy 7050 should be used with an extrusion ratio of at least 3% [25]. Figure 15 shows the residual stress distribution under different paths for extrusion ratios (P = 4 GPa) of 3%, 4%, 5%, and 6%; the influence of the change in extrusion ratio on the residual stress at the hole corner is further reduced, and the residual compressive stress in the hole corner area is "controlled" by laser peening, but the residual compressive stress in the middle area of the hole has a tendency to increase gradually, which is due to the fact that the reinforcement of LSP is limited in the direction of the depth of the material, and the residual stress distribution curve in the middle area of the hole wall is a "double camel peak", which does not change with the overall trend of the extrusion ratio.

From Figure 15, it can be observed that LUE-1 can achieve a favorable residual stress distribution in small holes at an extrusion ratio of 3%. With other parameters held constant, in the LUE-1 process, the change in residual compressive stress in the hole corner region is not significant with increasing extrusion ratio, while there is an increasing trend in the residual compressive stress values in the middle region of the hole. Therefore, the LUE-1 treatment of small-hole components should be combined with the appropriate extrusion ratio. If the extrusion ratio is too low, the strengthening effect will not be ideal. Although an increase in the extrusion ratio can improve the distribution of stress, if the actual production of the extrusion ratio is too large, it may lead to hole angle deformation [26].

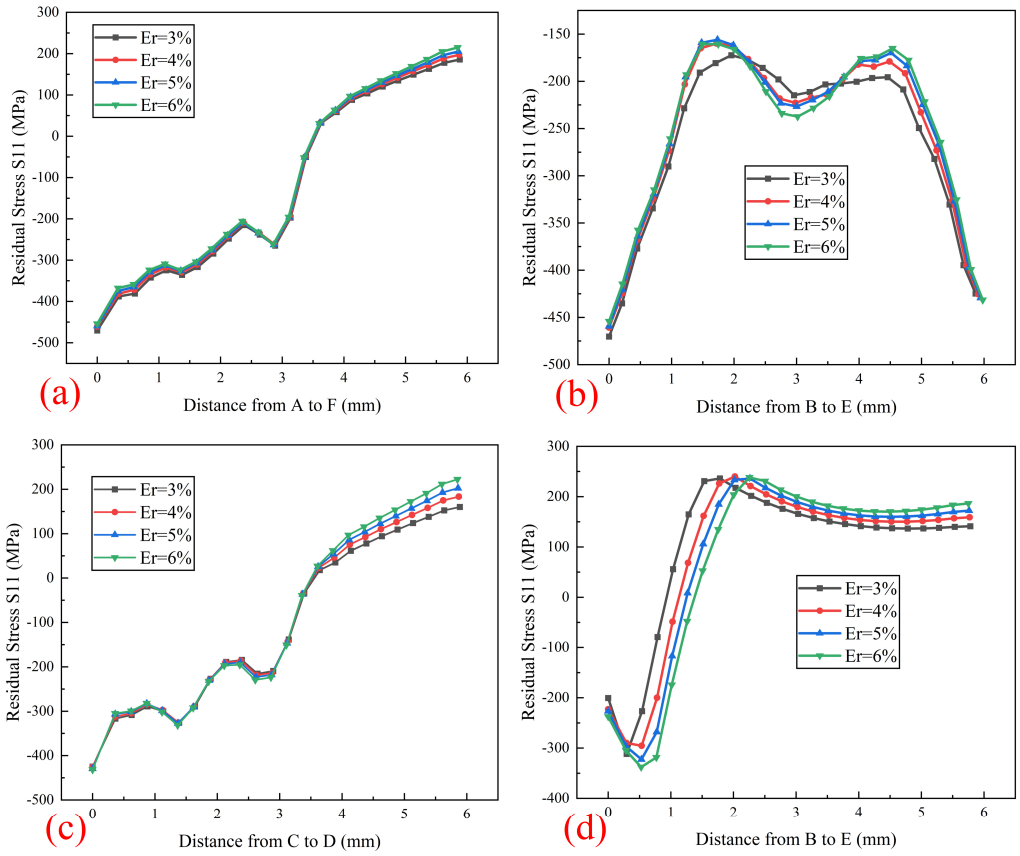

Figure 15. Simulation results of stress distribution of LUE-1 under different extrusion ratios (P = 4 GPa): (**a**) extrusion-inlet surface; (**b**) hole wall path; (**c**) extrusion-outlet surface; and (**d**) hole wall middle radial path.

3.5. Fatigue Test Results and Analysis

The optimized parameters from the previous simulation were selected for LUE-1 testing, with a P of 2.6 GPa, an extrusion ratio of 3%, and an amplitude of 8 μm. Then, fatigue tests were conducted to verify the accuracy of the simulated residual stress distribution

through the crack source initiation location, and the effectiveness of LUE-1 strengthening was verified through fatigue life gains.

3.5.1. Comparison and Analysis of Fatigue Life

According to the fatigue test results shown in Table 4, the difference in the fatigue life of the untreated end specimens is not significant, ranging from 65,468 to 69,355, and the random factors during the test process can be ignored. When the peak pressure is 2.6 GPa, the number of cyclic loading cycles for the specimen after LSP treatment increases significantly, but the value is not too large, with a fatigue life gain of about 115%. When the peak pressure increases to 4.5 GPa, as indicated in Figure 10, it can be observed that at this point, the entire hole wall is under residual compressive stress, and the fatigue life gain also increases to 193.61%. The fatigue life gain of the LUE-1 strengthened specimens can reach 310.66%, nearly three times higher than that of LSP (P = 2.6 GPa) and about 60% higher than that of single LSP (P = 4.5 GPa), indicating that the LUE-1 process is beneficial for improving the fatigue life of small-hole specimens, validating the effectiveness of LUE-1 strengthening.

Table 4. Result of fatigue test.

Sample No.	Strengthening Process	P/GPa	Untreated End Life/N1	Increased Life/N2	Treated End Life N1 + N2	Fatigue Life Gain N2/N1
1	LSP	2.6	65,468	72,519	137,987	110.77%
2	LSP	2.6	67,145	79,594	146,739	118.54%
3	LSP	4.5	67,855	131,374	199,229	193.61%
4	LUE-1	2.6	69,355	215,455	284,810	310.66%
5	LUE-1	2.6	68,539	211,457	279,996	308.52%

3.5.2. Macroscope Fractography

The fatigue fracture surface of the material is divided into three parts: the fatigue crack initiation (FCI) zone, the fatigue crack growth (FCG) zone, and the final rupture zone. In Figure 16, the red circle represents the fatigue crack initiation position, while the portion to the left of the red dashed line indicates the fatigue crack propagation zone, characterized by fatigue striations. The darker area represents the instantaneous fracture zone, which is characterized by the presence of dimples. Figure 16a shows the fatigue fracture surface without any strengthening. Stress concentration is significant at the void tips, and combined with numerous surface defects and low grain boundary binding, slip between grains is likely to occur. However, internal grain boundary restraint is sufficient, resulting in minimal defects within the metal body, making the crack initiation likely to occur in the void corner region. Figure 16b depicts the fatigue fracture surface after LSP. Both sides are affected by laser shock, resulting in the formation of high-density dislocations and finer grains on the material surface, which, to some extent, suppresses the initiation of surface cracks [27,28]. The crack source is driven from the hole corner surface to the middle of the hole wall.

Figure 16c shows the fatigue fracture surface after LUE-1. LUE-1 induces strengthening layers on both the hole corner surface and the axial direction of the hole wall. However, due to the action of laser peening at the end of the LUE-1 process, its effect predominates in the hole corner area, overcoming the problem of fatigue source appearing at the hole corner of the extrusion-inlet after cold extrusion strengthening [29,30]. Therefore, the crack source still exists in the middle of the hole, which also essentially verifies the residual stress distribution of a “double camel peak” in the hole wall in the previous simulation, with minimum residual stress in the middle of the hole wall (corresponding to the position where the crack source initiates in Figure 16c). The residual stress at the hole corner is relatively larger than that in the middle of the hole wall.

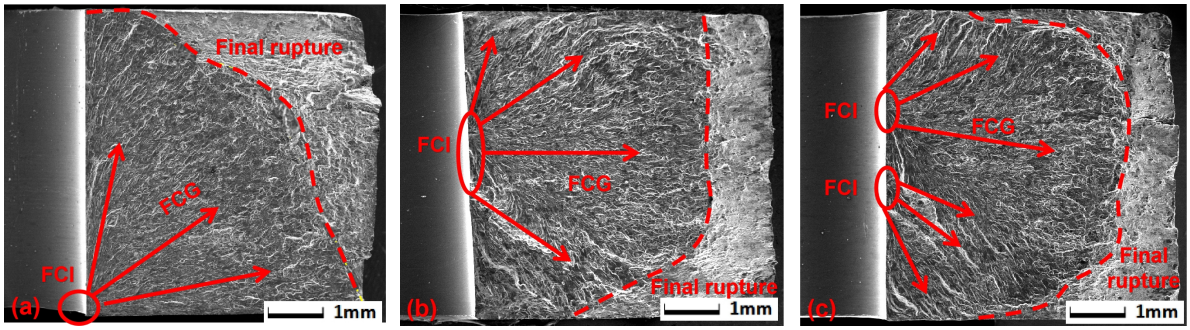

Figure 16. Macroscopic fracture comparison: (**a**) untreated; (**b**) LSP; and (**c**) LUE-1.

4. Discussion

Figure 17 shows the mechanism of LUE strengthening. As shown in Figure 17a, when LSP is applied to strengthen a small hole, a certain depth of strengthening layer is formed on the upper and lower surfaces of the hole. The hole corner at the extrusion-inlet and extrusion-outlet surface is strengthened, while a tensile stress zone exists in the middle of the hole wall, leading to the initiation of failure at the middle of the hole wall, where crack sources originate. In Figure 17b, when UES is used to strengthen a small hole, the extrusion of the mandrel onto the hole wall not only causes plastic deformation but also triggers plastic flow. Plastic flow refers to the continuous, irreversible deformation that occurs in a material under a sufficiently large shear stress, often accompanied by material flow. During the UES process of strengthening small holes, a portion of the material at the hole corner of the extrusion-inlet surface is pressed to other locations of the hole along the extrusion direction, resulting in tensile stress at the hole corner of the extrusion-inlet surface, leading to frequent fracture failure at the hole corner of the extrusion-inlet surface.

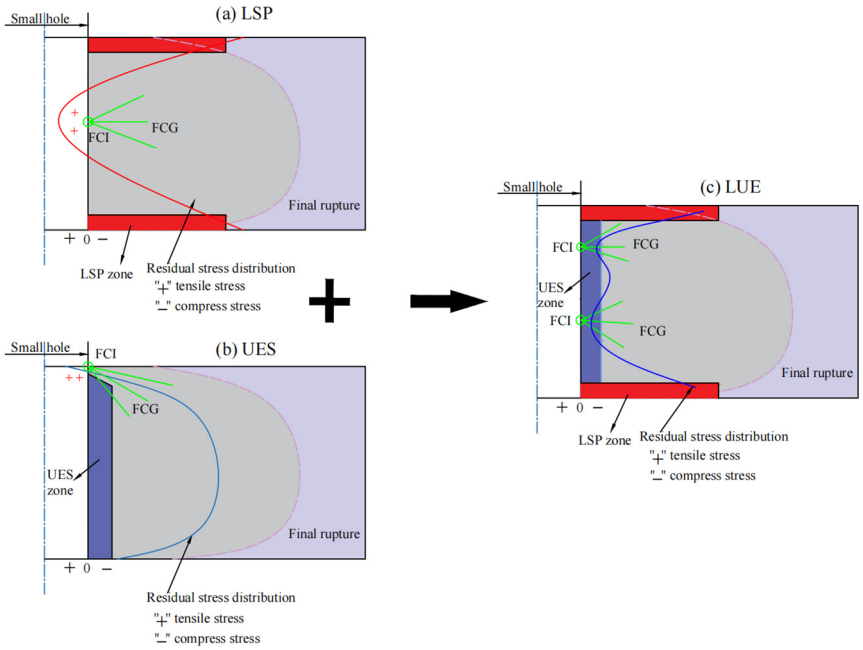

Figure 17. Schematic diagram of LUE strengthening mechanism.

In contrast, LUE introduces residual compressive stress throughout the hole wall, strengthening both the inner wall and the hole corners. Therefore, compared to LSP and UES, the ability of LUE specimens to prevent fatigue failure is stronger, and the fatigue life is longer. During fatigue failure, the initiation of cracks at the middle of the hole wall is

because the compressive stress in the middle of the hole wall is relatively smaller compared to other regions, consistent with the simulation results mentioned earlier.

5. Conclusions

The present study utilized the ABAQUS 6.14 finite element software to simulate the LUE process for strengthening the small-hole structure in aluminum alloy. It analyzed the effects of process factors (LUE process methods, peak pressure of laser, amplitude of ultrasonic extrusion, and extrusion ratio) on the residual stress distribution of the strengthened hole component. After selecting optimized parameters for experimentation, verifying the accuracy of residual stress distribution in simulations through crack initiation location, and verifying the effectiveness of LUE strengthening through fatigue life gain, the following conclusions are drawn:

1. When UES strengthening is performed, the material undergoes plastic deformation under the action of the mandrel, and the material at the extrusion-inlet surface is squeezed into the interior of the hole, while the material at the extrusion-inlet surface is strongly squeezed by the mandrel, which generates residual tensile stresses. When the process method of LUE is LUE-1, laser peening removes the tensile stresses in the hole corner of the extrusion-inlet surface. Therefore, during the LUE strengthening process, the optimal processing sequence involves perforating the sample first, followed by ultrasonic extrusion, and finally incorporating an anti-deformation mandrel for laser peening.

2. The increase in peak pressure will enhance the effect of laser peening in the LUE-1 process, causing the residual stress curve on the hole wall to gradually change from a "double camel peak" to a "convex peak". The compressive stress generated in the middle part of the hole wall due to ultrasonic extrusion will gradually be counteracted by the tensile stress brought about by laser peening. Compared to LSP, LUE-1 can generate better residual tensile stress on the entire hole wall under smaller peak pressures, which eliminates the thickness effect caused by LSP.

3. The amplitude significantly influences the mechanical characteristics during the LUE-1 process. As the amplitude increases, friction gradually decreases, while the fluctuation amplitude of friction increases. Although the amplitude variation affects the residual stress distribution of the small-hole structure after LUE-1, its impact is relatively minor.

4. Due to LSP's control over the hole corner, the extrusion ratio primarily affects the residual stress in the middle part of the small hole. An increase in the extrusion ratio leads to an increase in the residual compressive stress value in the middle part of the small hole. However, in actual production, an appropriate extrusion ratio should be selected according to the requirements as an excessively large extrusion ratio can cause deformation of the hole corner.

5. The fatigue life gain of the LUE-1-strengthened specimens can reach 310.66%, nearly three times higher than that of single LSP (P = 2.6 GPa) and about 60% higher than that of single LSP (P = 4.5 GPa), indicating that the LUE-1 process is beneficial for improving the fatigue life of small-hole specimens.

Author Contributions: Conceptualization, Y.J.; methodology, Y.J.; software, X.L., W.L. and Y.W.; validation, X.L. and Y.J.; formal analysis, Y.J. and L.C.; investigation, X.L., W.L., Y.W. and G.J.; resources, W.L., L.C. and G.J.; data curation, X.L., W.L. and Y.W.; writing—original draft preparation, X.L., Y.W. and W.L.; writing—review and editing, X.L., W.L., Y.W., G.J., Y.J. and L.C.; supervision, G.J., Y.J. and L.C.; project administration, Y.J. and G.J.; funding acquisition, Y.J. All authors have read and agreed to the published version of the manuscript.

Funding: This work was supported by the National Natural Science Foundation of China (No. 51075193) and the Project of Laser Processing and Metal Additive Manufacturing Technology and Application (SKJ2023-3).

Data Availability Statement: The original contributions presented in the study are included in the article, further inquiries can be directed to the corresponding authors.

Acknowledgments: We thank the National Natural Science Foundation of China for financial support.

Conflicts of Interest: The authors declare no conflicts of interest.

References

1. Chakherlou, T.; Aghdam, A.; Akbari, A.; Saeedi, K. Analysis of cold expanded fastener holes subjected to short time creep: Finite element modelling and fatigue tests. *Mater. Des.* **2010**, *31*, 2858–2866. [CrossRef]
2. Zhang, X.; Chen, L.; Yu, X.; Zuo, L.; Zhou, Y. Effect of laser shock processing on fatigue life of fastener hole. *Trans. Nonferrous Met. Soc. China* **2014**, *24*, 969–974. [CrossRef]
3. Chakherlou, T.; Vogwell, J. The effect of cold expansion on improving the fatigue life of fastener holes. *Eng. Fail. Anal.* **2003**, *10*, 13–24. [CrossRef]
4. Liu, H.; Hu, D.; Wang, R.; Wang, X.; Jin, S.; Gu, Y. Experimental and numerical investigations on the influence of cold expansion on low cycle fatigue life of bolt holes in aeroengine superalloy disk at elevated temperature. *Int. J. Fatigue* **2020**, *132*, 105390. [CrossRef]
5. Fu, Y.; Ge, E.; Su, H.; Xu, J.; Li, R. Cold expansion technology of connection holes in aircraft structures: A review and prospect. *Chin. J. Aeronaut.* **2015**, *28*, 961–973. [CrossRef]
6. Zheng, G.; Cao, Z.; Wang, Y.; Talemi, R. Fatigue response of open hole plates: A finite element simulation investigating the influence of dynamic and static cold expansion processes. *Finite Elem. Anal. Des.* **2024**, *230*, 104085. [CrossRef]
7. Shamdani, A.H.; Khoddam, S. A comparative numerical study of combined cold expansion and local torsion on fastener holes. *Fatigue Fract. Eng. Mater. Struct.* **2012**, *35*, 918–928. [CrossRef]
8. Liu, Y.; Liu, J.; Shao, X. Study on the residual stress fields, surface quality, and fatigue performance of cold expansion hole. *Mater. Manuf. Process.* **2011**, *26*, 294–303. [CrossRef]
9. Liu, Y.; Geng, D.; Shao, Z.; Zhou, Z.; Jiang, X.; Zhang, D. A study on strengthening and machining integrated ultrasonic peening drilling of Ti-6Al-4V. *Mater. Des.* **2021**, *212*, 110238. [CrossRef]
10. Han, G.; Wan, W.; Zhang, Z.; Xu, L.; Liu, F.; Zhang, H. Experimental investigation into effects of different ultrasonic vibration modes in micro-extrusion process. *J. Manuf. Process.* **2021**, *67*, 427–437. [CrossRef]
11. Mousavi, S.A.; Feizi, H.; Madoliat, R. Investigations on the effects of ultrasonic vibrations in the extrusion process. *J. Mater. Process. Technol.* **2007**, *187–188*, 657–661. [CrossRef]
12. Deng, W.; Wang, C.; Lu, H.; Meng, X.; Wang, Z.; Lv, J.; Luo, K.; Lu, J. Progressive developments, challenges and future trends in laser shock peening of metallic materials and alloys: A comprehensive review. *Int. J. Mach. Tools Manuf.* **2023**, *191*, 104061. [CrossRef]
13. Thiruneelakandan, R.; Balamurugan, R.; Prakasam, R. Improvised surface property of Al-7075 alloy by laser shock peening technique. *Mater. Today Proc.* **2023**, *92*, 1597–1601. [CrossRef]
14. Zheng, X.; Luo, P.; Yue, G.; Hu, Y. Analysis of microstructure and high-temperature tensile properties of 2060 Al-Li alloy strengthened by laser shock peening. *J. Alloys Compd.* **2021**, *860*, 158539. [CrossRef]
15. Sun, R.; Che, Z.; Cao, Z.; Zhang, H.; Zou, S.; Wu, J.; Guo, W. Effect of laser shock peening on high cycle fatigue failure of bolt connected AA2024-T351 hole structures. *Eng. Fail. Anal.* **2022**, *141*, 106625. [CrossRef]
16. Kashaev, N.; Ventzke, V.; Horstmann, M.; Chupakhin, S.; Riekehr, S.; Falck, R.; Maawad, E.; Staron, P.; Schell, N.; Huber, N. Effects of laser shock peening on the microstructure and fatigue crack propagation behaviour of thin AA2024 specimens. *Int. J. Fatigue* **2017**, *98*, 223–233. [CrossRef]
17. Gu, C.; Su, M.; Tian, Z.; Zhao, J.; Wang, Y. Multi-scale simulation study on the evolution of stress waves and dislocations in Ti alloy during laser shock peening processing. *Opt. Laser Technol.* **2023**, *165*, 109629. [CrossRef]
18. Jiang, Y.; Wang, S.; Jiang, W.; Gan, X.; Hua, C.; Qi, H.; Zhao, Y.; Huang, J. Fatigue life and fracture evolution of small-hole specimens by laser shock processing. *Opt. Laser Technol.* **2020**, *131*, 106423. [CrossRef]
19. Jiang, Y.; Li, X.; Jiang, W.; Wan, Q.; Gan, X.; Zhao, Y.; Hua, C.; Li, X.; Zhang, J. Thickness effect in laser shock processing for test specimens with a small hole under smaller laser power density. *Opt. Laser Technol.* **2019**, *114*, 127–134. [CrossRef]
20. Jiang, Y.; Wang, Y.; Sun, J.; Wu, G.; Jiang, W.; Liu, X.; Li, X. Study on the composite strengthening with laser shock processing and ultrasonic extrusion strengthening for small hole components. *Int. J. Fatigue* **2023**, *177*, 107908. [CrossRef]
21. Tang, C.; Li, H.; Li, K. Data-driven fatigue life prediction of small-deep holes in a nickel-based superalloy after a cold expansion process. *Int. J. Fatigue* **2024**, *181*, 108159. [CrossRef]
22. Achintha, M.; Nowell, D. Eigenstrain modelling of residual stresses generated by laser shock peening. *J. Mater. Process. Technol.* **2011**, *211*, 1091–1101. [CrossRef]
23. Amarchinta, H.K.; Grandhi, R.V.; Clauer, A.H.; Langer, K.; Stargel, D.S. Simulation of residual stress induced by a laser peening process through inverse optimization of material models. *J. Mater. Process. Technol.* **2010**, *210*, 1997–2006. [CrossRef]
24. Liu, F.; Su, H.; Liang, Y.; Xu, J. Fatigue performance on 7050 aluminum alloy by using ultrasonic vibration-assisted hole expansion strengthening. *Int. J. Adv. Manuf. Technol.* **2023**, *128*, 5153–5165. [CrossRef]
25. Li, Q.; Xue, Q.; Hu, Q.; Song, T.; Wang, Y.; Li, S.; Fu, F. Cold Expansion Strengthening of 7050 Aluminum Alloy Hole: Structure, Residual Stress, and Fatigue Life. *Int. J. Aerosp. Eng.* **2022**, *2022*, 4057898. [CrossRef]
26. Fu, S.; Wang, M.; Zuo, D.W. Prolonging fatigue life mechanism and test of coldworked hole. *Aeronaut. Manuf. Technol.* **1998**, *1*, 24–26.

27. Ren, X.; Zhan, Q.; Yang, H.; Dai, F.; Cui, C.; Sun, G.; Ruan, L. The effects of residual stress on fatigue behavior and crack propagation from laser shock processing-worked hole. *Mater. Des.* **2013**, *44*, 149–154. [CrossRef]
28. Zhang, Y.; Jian, X.; Xia, F. Effect of laser shock peening on surface integrity and tensile fatigue behavior of TB8 bolts. *Eng. Fail. Anal.* **2024**, *157*, 107968. [CrossRef]
29. Karabin, M.; Barlat, F.; Schultz, R. Numerical and experimental study of the cold expansion process in 7085 plate using a modified split sleeve. *J. Mater. Process. Technol.* **2007**, *189*, 45–57. [CrossRef]
30. Su, R.; Li, J.; Liu, W.; Xu, C.; Gao, L.; Liang, X.; Wu, D.; Huang, X.; Dong, H.; Ma, H. Investigation on fatigue failure of split-sleeve cold expansion holes of 7075-T651 aluminum alloy. *Mater. Today Commun.* **2023**, *35*, 106290. [CrossRef]

Disclaimer/Publisher's Note: The statements, opinions and data contained in all publications are solely those of the individual author(s) and contributor(s) and not of MDPI and/or the editor(s). MDPI and/or the editor(s) disclaim responsibility for any injury to people or property resulting from any ideas, methods, instructions or products referred to in the content.